Dynamic characteristics of wheelsets with a rail considering viscous-elastic properties of the material

Ahmedov O. [iD] [✉], Mirsaidov M. [iD]

Tashkent Institute of Irrigation and Agricultural Mechanization Engineers, National Research University,

Tashkent, Uzbekistan

✉ olimjon84@mail.ru

Abstract. Assessment of the dynamic characteristics (eigenfrequencies, modes and decrement of vibration) of rolling stock wheelsets is an urgent task. This study is devoted to the evaluation of the dynamic characteristics of wheelsets together with the rail taking into account the inelastic properties of the shaft material, wheel sliding, and rolling stock speed. A mathematical model for assessing the dynamic characteristics of wheelsets, taking into account the viscoelastic properties of the material of the system was developed using the Boltzmann-Volterra hereditary theory. A method and algorithm were developed to reduce the problem of natural oscillations of the system to an algebraic eigenvalue problem. Dynamic characteristics of the wheelsets were determined under various parameters of the viscoelasticity of the material. A mathematical model was developed to evaluate the dynamic characteristics of wheelsets with a rail, while considering dissipative processes and using a linear combination of mass and stiffness matrices of the system. Eigenfrequencies, modes and decrement of vibrations of rolling stock wheelsets with a rail were determined taking into account wheel sliding and rolling stock speed. Some mechanical effects were revealed.

Keywords: rolling stock, wheelsets, dynamic characteristics, viscoelasticity, adhesion, sliding, damping

Introduction

Important dynamic characteristics of wheelsets are the assessment of eigenfrequencies, modes of vibrations and damping coefficient considering energy dissipation in the material. These values actually characterize the degree of vulnerability of the structure to dynamic loads.

A number of publications deal mainly with the issues of numerical and experimental determination of the frequency spectrum of natural vibrations of wheelsets. The study in [1] proposes a numerical and experimental method for determining the eigenfrequency spectrum of wheelsets. The damping coefficients were experimentally found to range from 0.1 to 1.0 % for each frequency.

Reference [2] is devoted to solving the problem of oscillations for a rotating flexible wheelset taking into account the contact and flexibility of the wheelset, and the effect of rotation. Flexible modes of vibrations with frequencies less than 1000 Hz and proportional damping coefficients for all frequencies within 0.2 % are taken into account.

The authors of [3] presented the analysis of natural frequencies spectrum of the traction wheelset and rail track obtained experimentally and by the three-dimensional finite element

method. At that, the eigenmodes are determined for eigenfrequencies, which correspond to the excitation frequency caused by the short pitch rail corrugation. The results show that the excitation frequency at the average speed of the train on curved tracks corresponds to the eigenfrequency of the wheelset. The results obtained by the FEM for wheelsets are in better agreement at a frequency of 100 Hz.

The study in [4] is devoted to the development of a new wheel/rail contact model to consider the effect of deformation under wheelset bending on the wheel/rail contact behavior at high speeds. In determining the frequency spectrum of high-speed rolling stock, two models of wheelset bending were considered, i.e., a model of rigid wheelsets, and a model of flexible wheelsets. Here, the wheelsets were modeled as the Euler-Bernoulli beam, and the wheel was considered rigid and always perpendicular to the deformed axis in the center of the wheel. The results obtained show that the proposed contact models characterize the effect of the first two wheelset bending modes on the contact behavior quite well.

In [5], three mathematical models based on the Euler approach were presented to obtain the dynamic characteristics of an elastic body of revolution that rotates around its principal axis at a constant angular velocity. The proposed models are related to the study of the interaction between a rigid body and a non-rotating system, i.e., to the study of the dynamics of a railway wheelset with a rail. The calculations performed using these models show the existence of a spectral deviation in the analysis of the Campbell diagram for a railway wheel. It should be noted that damping coefficients are not taken into account in this case.

Paper [7] presents the modeling of eigenfrequencies of flexible wheelsets on the track using the FEM. The obtained results of natural frequencies are compared with measurements on the track. The effect of structural flexibility of the wheelset on the travel forces in the frequency range of 0–100 Hz was studied. It was shown that both lateral and vertical caterpillar forces significantly depend on the flexibility of the wheelset, and they are in good agreement with the measurements. The flexibility of the wheelset increases the lateral forces of the track.

In [6], the effect of the flexibility of a wheelset design on the dynamics of the rolling stock was studied. The main attention was paid to the experimental and numerical spectral analysis of the locomotive wheelset in the frequency range of 0–500 Hz. The results of the numerical spectral analysis obtained are in good agreement with the results of the experiment. It was established that the wheelset has rather low natural frequencies.

Reference [8] is devoted to fundamental research related to the study of the influence of wheelset flexibility on the polygonization of locomotive wheels. Contact responses to track roughness for a free wheelset and a wheelset on the track were studied taking into account the effect of rotation; the influence of the wheelset flexibility on contact responses excited by white noise for straight and curved sections of tracks were investigated. The influence of the compliance of the wheelset on the development of polygonization of wheels was tested on the basis of the developed program. The results showed that the flexibility of a wheelset cannot dominate the polygonization of a railway wheel in a general sense. The torsion mode of the wheelset can be effectively excited by the spasmodic vibration due to the strong contact adhesion, which can take place on the track with small curvature radii or high traction moment.

In [9], using dynamic tests of the body and bogie of a rail car, 13 frequencies and modes of vibrations were determined at different vibration regimes using the method of stochastic identification of a subspace. In addition, dynamic testing of the systems of passenger seats was conducted. Model calibration was performed using a multi-stage modeling approach. The calibration was conducted by an iterative method based on a genetic algorithm and made it possible to obtain the optimal values of 17 parameters of the numerical model. A comparison of the experimental and numerical results before and after calibration revealed significant improvements in the numerical model and a very good correlation between the responses obtained with the calibrated model and experimental responses.

In [10], the problem of low-frequency oscillations of the cabin in the direction of translational motion during the operation of the vibratory roller was solved. A spectral test was conducted for a single drum vibratory roller to determine the natural frequency of the railway vehicle. The results of the FEM simulation led to a good agreement between the results and experiments. The design parameters of the cabin isolation system were optimized to ensure maximum avoidance of resonant vibration of a cabin.

In [11], a model of a railway vehicle wheelset was proposed, which takes into account the flexibility of the wheelset to study dynamic stability. The parameters corresponding to the wheelset flexibility were analyzed; they have the greatest influence on the critical speed of high-speed vehicles and vehicles with a variable gauge.

In [12], field tests and numerical simulations of the formation mechanism and key factors affecting the high-order polygonization of a wheel were conducted. Experimental results showed that polygonization of wheels is associated with the first-order bending vibration of the wheelset and the P2 resonance that occurs on tracks with staircase sleepers and floating plates. To investigate the causes of wheel polygonization, a long-term wear model was developed that included a dynamic model associated with the vehicle and track considering the flexibility of the wheelset and track. The influence of operating speeds, resonant frequencies P2 for various tracks and the flexibility of wheelsets on the development of wheel polygonization were investigated. Based on the results of experiments and simulations, it was further assumed that the P2 resonance is the main cause of high-order polygonal wear of wheels, and the first-order bending vibration of the wheelset can exacerbate wheel polygonization.

The study in [13] describes a procedure for numerical and experimental design, which makes it possible to soften the resonance of a loco wheel under radial and lateral excitations through viscoelastic layers. It was proven that these high frequencies could be reduced by proper design of the damping layer mechanisms. Visco-elastic damping layers were analyzed. The results showed that the correct design and dimensions of viscoelastic damping layers successfully reduced the high amplitude resonant peaks of the wheel under radial and lateral excitations.

In [14], railway wheelsets were considered in modeling as a one-dimensional deformable body based on the Bernoulli-Euler theory with two rigid discs. The discs were modeled as a rigid body characterized by mass and moment of inertia. This takes into account the centrifugal and gyroscopic effects and the damping properties of the material. Taking these factors into account, the problem under consideration was reduced to a high-order homogeneous system of differential equations. The dynamic characteristics of railway wheelsets were studied depending on the angular velocity of the wheel (without considering the wheelset/rail contact) under simple damping.

Reference [15] is devoted to the study of the vibration wave propagation caused by railway transport and the assessment of its levels at various objects. In that study, using a variational approach, a mathematical model was developed to describe vibration wave propagation from railway transport over various distances. A technique for solving the considered problems using the finite element method was developed. The level of vibrations propagating from the railway transport motion to buildings located at a certain distance from the source of vibrations was studied.

Recently, the Boltzmann–Volterra hereditary theory of viscoelasticity has been increasingly used to describe the damping properties of the material [16–20,26]. When studying natural vibrations of various deformable systems using this theory, it is possible to determine the complex natural frequencies of the system; the real part of it shows the oscillation frequency, and the complex part shows the damping coefficient of the system.

This concludes our overview of some of the publications devoted to solving various dynamic problems of railway wheelsets with or without damping.

Each of these approaches, when solving specific problems, has its advantages and disadvantages, however, all of them are used in solving practical problems.

This review shows the incompleteness of research in determining the dynamic characteristics (natural frequencies, modes and damping coefficient) of wheelsets taking into account the viscoelastic properties of the material.

Therefore, this study is devoted to the development of mathematical models and the method for assessing the dynamic characteristics of wheelsets taking into account viscoelastic damping, which is an urgent problem.

Methods

Mathematical model. All materials exhibit some viscoelastic properties. In well-known metals such as steel, and aluminum the behavior at room temperature and under light load does not deviate much from linear elasticity. Under certain conditions, even a small viscoelastic response can be significant. Therefore, when compiling mathematical models of real structures or systems, it is necessary to take into account the viscoelastic properties of the material.

We consider railway wheelsets mounted on two bearings (radiaxial and radial ones) and consisting of a hollow shaft and two discs (Fig. 1).
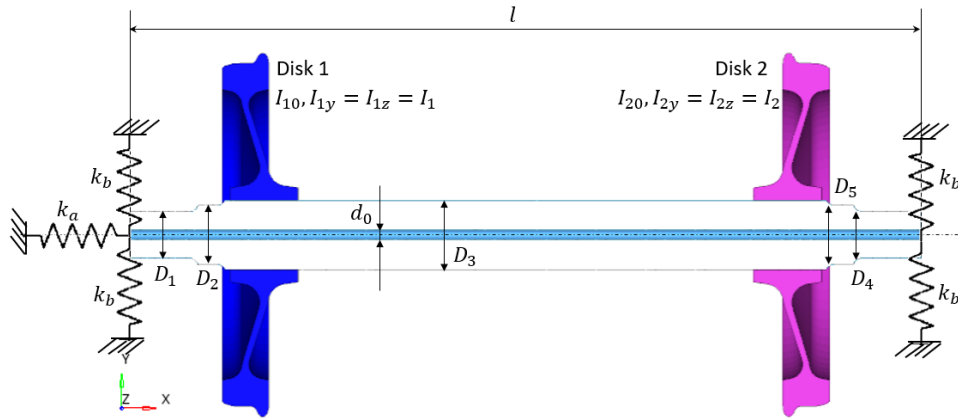

Fig. 1. Calculation scheme of a railway wheelset

In modeling the wheelset is considered as a one-dimensional deformable body based on the Bernoulli-Euler theory with two rigid discs. The cross-section of the shaft is assumed flat and perpendicular to the centerline under vibration. Discs are modeled as rigid bodies characterized by mass and moment of inertia [14].

The wheelset (Fig. 1) is considered a non-conservative system for which it is necessary to determine the dynamic characteristics (i.e., natural frequencies, modes, and damping factor).

For the mathematical formulation of the problem under consideration, the Lagrange equations for the shaft (without external excitation) are used in a matrix form

$$\frac{d}{dt}\left(\frac{\partial E_k}{\partial \dot{q}}\right) - \left(\frac{\partial E_k}{\partial q}\right) + \left(\frac{\partial E_p}{\partial q}\right) = 0. \tag{1}$$

The problem under consideration is solved by the finite element method, so the kinetic E_k and potential E_p energy of the system (Fig. 1) can be written as:

$$E_k = \sum_{e=1}^{N} E_k^{(e)}, E_p = \sum_{e=1}^{N} E_p^{(e)}. \tag{2}$$

Here, $E_k^{(e)}, E_p^{(e)}$ are the kinetic and potential energies for the eth finite element; N is the number of finite elements the considered shaft is partitioned into.

To determine expression (2) in explicit form, a one-dimensional eth finite element of circular cross-section is selected from the shaft as a finite element [14]. At that, deformations of the finite element at any point x are described by deflections $u(x)$ (in the x direction), $v(x)$ (in the y direction), $w(x)$ (in the z direction), Euler angles of rotation of the section plane $\vartheta(x)$,

$\psi(x)$ and torsional rotation $\varphi(x)$. It is assumed that the section plane after deformation remains perpendicular to the axis of the deformable shaft.

To describe the damping properties of the shaft material, according to [16–20], the Boltzmann-Volterra hereditary theory of viscoelasticity is used. The viscous-elastic properties of the shaft material are described by an integral operator of the following form

$$\left. \begin{aligned} \tilde{E}[\varphi(t)] &= E\left[\varphi(t) - \int_0^t \Gamma_E\,(t-\tau)\varphi(t)d\tau\right] \\ \tilde{G}[\varphi(t)] &= G\left[\varphi(t) - \int_0^t \Gamma_G\,(t-\tau)\varphi(t)d\tau\right] \end{aligned} \right\}. \tag{3}$$

Here, E and G are the instantaneous moduli of elasticity of the material under tension (compression) and shear, respectively; Γ_E, Γ_G are the relaxation kernels; $\varphi(t)$ is an arbitrary function of time.

For the *e*th finite element, the matrices of stiffness and mass have the following form [14]:

$$\overline{K}^{(e)} = \begin{bmatrix} S_1^{-T}\overline{I}_3 S_1^{-1} & 0 & 0 & 0 \\ 0 & S_2^{-T}\overline{I}_3 S_2^{-1} & 0 & 0 \\ 0 & 0 & S_3^{-T}\overline{I}_6 S_3^{-1} & 0 \\ 0 & 0 & 0 & S_3^{-T}\overline{I}_7 S_3^{-1} \end{bmatrix}. \tag{4}$$

The coefficients of matrix (1.4) are complex values since $\overline{I}_3, \overline{I}_6, \overline{I}_7$ are matrices with complex parameters.

Let us assume that the integral terms in (1.3) are small in comparison with an arbitrary function of time $\varphi(t)$ and

$$\varphi(t) = \psi(t)e^{-i\omega_R t}, \tag{5}$$

where ψ is a slowly varying function of time, i is an imaginary unit, ω_R is a real constant.

Using the freezing method [16,17,19,21,22], one can replace (3) with the following complex expression:

$$\left. \begin{aligned} \tilde{E}[\varphi(t)] &\approx \overline{E}[\varphi(t)] = E[1 - \Gamma_E^c(\omega_R) - i\Gamma_E^s(\omega_R)]\varphi(t) \\ \tilde{G}[\varphi(t)] &\approx \overline{G}[\varphi(t)] = G[1 - \Gamma_G^c(\omega_R) - i\Gamma_G^s(\omega_R)]\varphi(t) \end{aligned} \right\}, \tag{6}$$

here,

$$\Gamma_E^c(\omega_R) = \int_0^\infty \Gamma_E\,(\tau)\cos\omega_R\,\tau d\tau, \ \ \Gamma_E^s(\omega_R) = \int_0^\infty \Gamma_E\,(\tau)\sin\omega_R\,\tau d\tau, \tag{7}$$

$$\Gamma_G^c(\omega_R) = \int_0^\infty \Gamma_G(\tau)\cos\omega_R\,\tau d\tau, \Gamma_G^s(\omega_R) = \int_0^\infty \Gamma_G(\tau)\sin\omega_R\,\tau d\tau, \tag{8}$$

where $\Gamma_E^S, \Gamma_E^C, \Gamma_G^S, \Gamma_G^C$ are the sines and cosines of the Fourier image of kernel $\Gamma_E(\tau), \Gamma_G(\tau)$.

Therefore, the elements of matrix (4) take the following form:

$$S_1 = \begin{bmatrix} 1 & 0 & 0 & 0 \\ 0 & 1 & 0 & 0 \\ 1 & l & l^2 & l^3 \\ 0 & 1 & 2l & 3l^2 \end{bmatrix}, \qquad S_2 = \begin{bmatrix} 1 & 0 & 0 & 0 \\ 0 & -1 & 0 & 0 \\ 1 & l & l^2 & l^3 \\ 0 & -1 & -2l & -3l^2 \end{bmatrix}, \qquad S_3 = \begin{bmatrix} 1 & 0 \\ 1 & l \end{bmatrix}, \tag{9}$$

where l denotes the length of the finite element of the shaft.

In the case of a prismatic section of the element, the area $A(x) = A$, the quadratic moments of inertia $J(x) = J$, and the polar moment $J_p = 2J$ are constant along the entire length

$$I_1 = \varrho A l \begin{bmatrix} 1 & l/2 & l^2/3 & l^3/4 \\ l/2 & l^2/3 & l^3/4 & l^4/5 \\ l^2/3 & l^3/4 & l^4/5 & l^5/6 \\ l^3/4 & l^4/5 & l^5/6 & l^6/7 \end{bmatrix}, \qquad I_2 = \varrho J l \begin{bmatrix} 0 & 0 & 0 & 0 \\ 0 & 1 & l & l^2 \\ 0 & l & 4l^2/3 & 3l^3/2 \\ 0 & l^2 & 3l^3/2 & 9l^4/5 \end{bmatrix},$$

$$\overline{I}_3 = \overline{E} J l \begin{bmatrix} 0 & 0 & 0 & 0 \\ 0 & 0 & 0 & 0 \\ 0 & 0 & 4 & 6l \\ 0 & 0 & 6l & 12l^2 \end{bmatrix}, \qquad I_4 = \varrho A l \begin{bmatrix} 1 & l/2 \\ l/2 & l^2/3 \end{bmatrix}, \qquad I_5 = \varrho J_p l \begin{bmatrix} 1 & l/2 \\ l/2 & l^2/3 \end{bmatrix},$$

$$\bar{I}_6 = \bar{E}Al \begin{bmatrix} 0 & 0 \\ 0 & 1 \end{bmatrix}, \qquad\qquad \bar{I}_7 = \bar{G}J_p l \begin{bmatrix} 0 & 0 \\ 0 & 1 \end{bmatrix}, \qquad\qquad (10)$$

where ϱ is the density of the material.

As a result of the operations performed, we obtain mass matrix $\boldsymbol{M}^{(e)}$, matrix of gyroscopic effects $\boldsymbol{G}^{(e)}$ and stiffness matrix $\boldsymbol{K}^{(e)}$ (considering the energy dissipation in the material) for the eth finite element.

The procedure of the finite element method allows us to write the potential and kinetic energy (1.2) for the system under consideration (Fig. 1) in the following form:

$$E_k = \sum_{e=1}^{N} E_k^{(e)} = \frac{1}{2} \boldsymbol{q}^T \boldsymbol{M} \dot{\boldsymbol{q}} + \omega_0 (\dot{\boldsymbol{q}})^T \boldsymbol{C} \boldsymbol{q} + \frac{1}{2} \omega_0^2 (\boldsymbol{q})^T \boldsymbol{K}_d \boldsymbol{q} + \omega_0 (\dot{\boldsymbol{q}})^T \boldsymbol{f}_1 + \frac{1}{2} \omega_0^2 I$$

$$E_p = \sum_{e=1}^{N} E_p^{(e)} = \frac{1}{2} (\boldsymbol{q})^T \boldsymbol{K}_s \boldsymbol{q}. \qquad\qquad (11)$$

Substituting the expression for kinetic and potential energy (11) into the Lagrange equation (1), we obtain a system of homogeneous ordinary differential equations in a matrix form that describes the natural vibrations of a rotating shaft, i.e.:

$$\boldsymbol{M}\ddot{\boldsymbol{q}}(t) + \omega_0 \boldsymbol{G}\dot{\boldsymbol{q}}(t) + (\boldsymbol{K}_s - \omega_0^2 \boldsymbol{K}_d)\boldsymbol{q}(t) = \boldsymbol{0}. \qquad\qquad (12)$$

Here: $\boldsymbol{M}$ is the global mass matrix, $\boldsymbol{C}$ is the global Coriolis matrix, $\boldsymbol{f}_1$ is the global vector of gyroscopic forces, I is the total moment of inertia of the shaft around the x-axis, $\boldsymbol{K}_d$ is the global matrix of rotation softening, $\boldsymbol{K}_s$ is the global static stiffness matrix with complex coefficients, $\omega_0 \boldsymbol{G} = \omega_0 (\boldsymbol{C} - \boldsymbol{C}^T)$ is the global matrix of gyroscopic effects.

The matrix of the global vector of node deviation (i.e., the vector of coordinates of the generalized system) has the following form:

$$\boldsymbol{q} = [\boldsymbol{q}_i], \quad \boldsymbol{q}_i = [u(x), v(x), w(x), \varphi(x), \vartheta(x), \psi(x)]^T, \quad i = 1, 2, \ldots, N, N+1 \qquad (13)$$

Now it is necessary to determine the natural oscillations, i.e. the most ordered movement of the system (Fig. 1), occurring in the absence of external influences; all points of the system oscillate according to the same complex harmonic law but at different amplitudes.

Solution method. To determine the dynamic characteristics of the system (Fig. 1), it is necessary to find a non-trivial solution of equation (12) in the following form

$$\boldsymbol{q}(t) = \boldsymbol{q}^* e^{-i\omega t}, \qquad\qquad (14)$$

Here, the real part of the complex natural frequency $\omega = \omega_R - i\omega_I$ means the oscillation frequency, and the imaginary part determines the damping rate of the system oscillations (Fig. 1) and has the meaning of the damping coefficient.

Substitution of (14) into (12) reduces the problem under consideration to a complex algebraic eigenvalue problem, i.e.:

$$([(\boldsymbol{K}_s - \omega_0^2 \boldsymbol{K}_d) - \omega_0 \omega \boldsymbol{G} + \omega^2 \boldsymbol{M})])\boldsymbol{q}^* = 0. \qquad\qquad (15)$$

Here, $\boldsymbol{K}_s$ is a complex stiffness matrix; the values of its elements depend on the sought-for parameter ω_R; $\omega = \omega_R - i\omega_I$ is the complex eigenfrequency, and $\boldsymbol{q}^*$ is the complex eigenvector corresponding to the eigenfrequencies ω of the system.

The order of the system of algebraic eigenvalue equations (15) reaches 200. They are solved by the Matlab software using the eig function.

The method described above was used to evaluate the dynamic characteristics of the steel shaft of railway wheelsets mounted on two bearings (radiaxial and radial ones). Wheelsets consist of a hollow shaft and two discs (Fig. 1). To take into account the energy dissipation in the material of the shaft, the Boltzmann-Volterra hereditary theory of viscoelasticity was used.

The following geometric and physico-mechanical parameters of wheelsets were used for specific calculations: shaft inner diameter d_{shaft}=0.026 m; shaft outer diameters D_1=0.13 m, $D_2 = 0.165$ m, $D_3 = 0.194$ m, $D_4 = 0.1475$ m, $D_5 = 0.179$ m; shaft length $l = 2.216$ m; bearing stiffness $k_b = 6e + 12$ [N/m], $k_a = 2e + 12$ [N/m]; moment of inertia of discs $I_{10} = I_{20} = 54.69$ kg · m^2, $I_1 = I_2 = 27.88$ kg · m^2; disc mass $m_1 = m_2 = 364.57$ kg, shaft material

properties: modulus of elasticity $E = 2.1e+11$ Pa, $G = 8.076e+10$ Pa; Poisson's ratio $\nu = 0.30$; material density $\rho = 7850$ kg /m^3.

Further, this problem is solved by taking into account the viscoelastic properties of the material. The accuracy of solutions depends on the correct choice of the relaxation kernel. The accuracy of kernel approximations should be verified by comparing them with experimental curves. The existing Koltunov–Rzhanitsyn three-parameter singular hereditary kernels satisfy all the conditions imposed on the creep and relaxation kernel and best approximate the experimental data over a long period. Therefore, the Koltunov–Rzhanitsyn three-parameter kernels [17-19] are used as the relaxation kernels in the integral operator (3) in the following form

$$\Gamma(t) = Ae^{-\beta t}t^{\alpha-1} \tag{16}$$

Here, $\Gamma_E^S, \Gamma_E^C, \Gamma_G^S, \Gamma_G^C$ are the sines and cosines of the Fourier image of kernel $\Gamma_E(\tau), \Gamma_G(\tau)$ and are calculated by the following formulas

$$\Gamma_j^S = \frac{A\cdot\Gamma(\alpha)}{(\omega_i^2+\beta^2)^{\frac{\alpha}{2}}}\sin\left(\alpha\cdot\text{arctg}\frac{\omega_i}{\beta}\right), \qquad \Gamma_j^C = \frac{A\cdot\Gamma(\alpha)}{(\omega_i^2+\beta^2)^{\frac{\alpha}{2}}}\cos\left(\alpha\cdot\text{arctg}\frac{\omega_i}{\beta}\right),$$

$$\Gamma^* = A\cdot\Gamma(\alpha)/(\beta^\alpha), \tag{17}$$

where $\Gamma(\alpha)$ is the gamma function, α $(0 < \alpha < 1)$ is the singularity parameter determined by experiment, β $(\beta > 0)$ is the damping parameter (constant coefficient), A is the viscosity parameter $(A > 0)$.

Results and discussion
Dynamic characteristics of wheelsets considering viscoelastic properties of the material.
In the dynamic analysis of viscoelastic mechanical systems, the real part of the eigenvalues corresponds to the eigenfrequencies of vibrations, and the eigenvectors characterize the eigenmodes of these vibrations. In the case of non-rotating wheelsets (i.e. for $\omega_0 = 0$ rad/s), considering the bearings, the equation of motion of the system has the following form:

$$(M + M_1^{(D)} + M_2^{(D)})\ddot{q}(t) + (\overline{K}_s + K_B)q(t) = 0, \tag{18}$$

where K_B is the matrix of bearing stiffness, $M_1^{(D)}, M_2^{(D)}$, and M – are the matrices of disc masses and the matrix of wheelset shaft masses, $\overline{K}_s$ is the stiffness matrix of wheelset shaft with complex coefficients.

Substituting (14) into (18), the problem of determining the generalized eigenvalue problem can be written as

$$\left[(\overline{K}_s + K_B) - \lambda\left(M + M_1^{(D)} + M_2^{(D)}\right)\right]q^* = 0, \tag{19}$$

where $\lambda = \omega^2, \omega = \omega_R - i\omega_I$.

This homogeneous complex algebraic equation (19) is a complex eigenvalue problem.

The eigenvalues λ of system (19) are complex quantities, i.e. and their real part ω_R is the eigenfrequencies of wheelsets in rad/s. The imaginary part of ω_I is the damping coefficients of the system by taking into account the viscoelastic properties of the material.

In the specific calculation of the kernel parameters (17), the values of $\alpha = 0.4$, $\beta = 0.05$ and $A = 0.1 \dots \dots 1$ were taken.

Table 1 shows the first eight eigenfrequencies $f_\nu = \omega/2\pi$ of a non-rotating wheelset obtained using the Matlab software considering the viscoelastic parameters of the material.

Table 1. Eigenfrequencies and oscillation decrement of non-rotating wheelsets for A = 0.35 and $\alpha = 0.4, \beta = 0.05$

Natural frequency numbers	Elastic material, Natural frequency f [Hz],	Viscoelastic material, Natural frequency $f = (\omega_R - i\omega_I)/2\pi$ [Hz],	Imaginary part i.e. Damping coefficients, D_v	Oscillation decrement $\delta = -2\pi\left(\frac{\omega_{Im}}{\omega_{Re}}\right)$
1	0	0	0	0
2,3	57.83	57.7054–0.0914i	0.0914	0.01
4	80.07	79.9007–0.1266i	0.1266	0.01
5,6	163.6	163.2249–0.2586i	0.2586	0.01
7,8	354.11	353.3671–0.5598i	0.5598	0.01

Analysis of the results obtained (Table 1) considering the viscoelastic properties of the material shows that for all complex frequencies, the real and imaginary parts change proportionally. This means that the logarithmic oscillation decrement is independent of the number of frequencies.

If the viscoelastic properties of the material are taken into account, the oscillation frequency ω_R slightly decreases. This is because the dynamic modulus of elasticity is less than the static modulus.

Then, the damping coefficients D_v were calculated depending on the viscosity parameter A for $\alpha = 0.4, \beta = 0.05$.

The results of these calculations, i.e. the dependence of the damping coefficients D_v of the wheelset on the viscosity parameter A are shown in Fig. 2.

An analysis of the results of the damping coefficient D_v dependence on the viscosity parameter A (Fig. 2) shows that the values of the damping coefficient increase linearly with increasing viscosity. At that, the greater the value of the oscillation frequency of the system, the greater the damping coefficient. This means that the higher modes of vibration attenuate much faster than the first modes of the system's vibrations. This is especially important for damping the vibrations of higher tones and is more pronounced in the resonant modes of the system's vibrations.
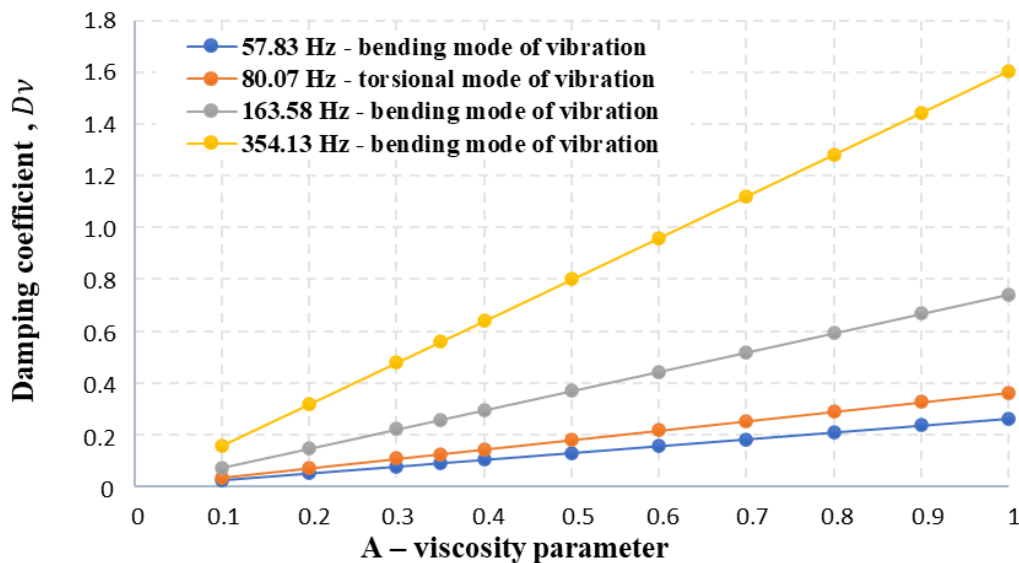

Fig. 2. Dependence of the damping coefficient on the viscosity parameter of the wheelset material

Dynamic characteristics of wheelsets with a rail. When controlling the wheel/rail relationship, it is shown that during the transfer of traction force there is always a certain difference between the angular velocity of the wheel $r\omega$ and its longitudinal speed v. If, as the difference increases, the friction coefficient also increases $\mu = \frac{T}{N}$, i.e., the ratio of the thrust force T to the normal force N or the magnitude of the thrust force, then the speed difference will be denoted as effective slip.

The value of traction is the difference in the speed of effective sliding. When the adhesion coefficient is exceeded, the sliding speed rapidly increases, the tangential force in the wheel contact decreases and slippage occurs. This means that the peak of the sliding characteristic corresponds to the adhesion coefficient. The dependence of the adhesion coefficient (or tensile force under a given normal load) on the so-called longitudinal relative sliding $s = \frac{r\omega - v}{v}$ is called wheel slippage on the rail. Therefore, the adhesion characteristic has the form shown in Fig. 3.

Usually, the adhesion coefficient and the shape of the sliding characteristic greatly depend on the current conditions. In general, when the adhesion coefficient decreases, the sliding speed corresponding to the maximum of the sliding characteristic is shifted to higher values. At that, the maximum of the trajectory is less pronounced. Under very poor adhesion conditions, the sliding characteristic may not have a maximum.

The adhesion coefficient μ in the wheel/rail contact is called the longitudinal adhesion coefficient, and it is determined experimentally. In [23], on the basis of the experiment, it was recommended to describe the adhesion coefficient μ depending on the relative sliding s and railway vehicle speed v in the following form:

$$\mu(s,v) = \frac{2}{\pi} f \left[arctg \left(\frac{s}{\rho_{adf}} \right) + \frac{\frac{s}{\rho_{adf}}}{1 + (\frac{s}{\rho_{adf}})^2} \right]. \tag{20}$$

In this case, the friction coefficient f (for the mode of wheels moving along the rail due to shear) is given by the following dependence:

$$f = a \cdot e^{-bvs} + c. \tag{21}$$

According to [23], constants a,b,c for normal conditions of contact between a wheel of a traction vehicle and a rail have the following values: $a = 0.395$, $b = 0.2083$, $c = 0.125$.
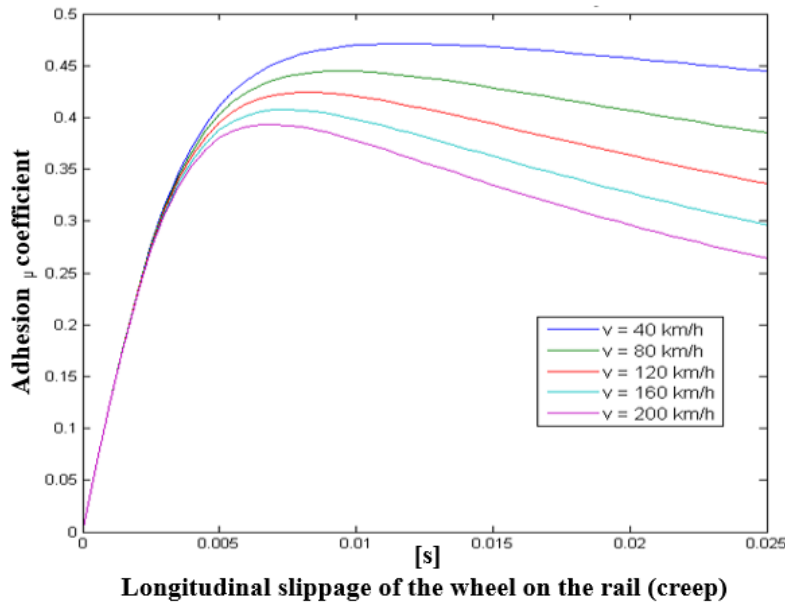

Fig. 3. Adhesion characteristics

The adhesion parameter ρ_{ad} depends on the maximum normal pressure, the radius of the longitudinal semi-axis of the contact surface and the constant expressing the elastic properties of the surfaces of the contacting bodies; based on this, it is proposed to take $\rho_{ad} = (5 \div 15) \cdot 10^{-3}$.

Figure 3 shows the adhesion characteristics for $\rho_{ad} = 10^{-2}$ and for different vehicle speeds $v = 40 \div 200 \, km/h$.
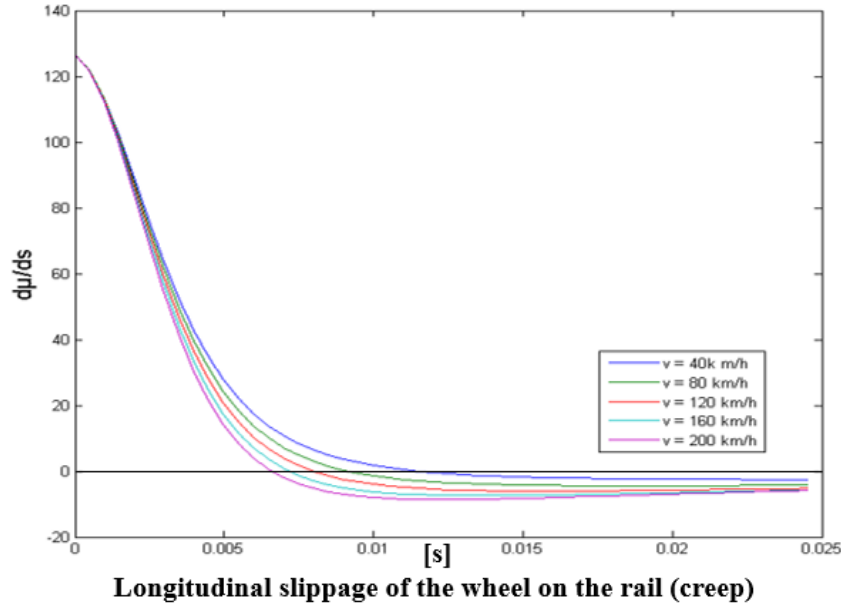

Fig. 4. Derivative adhesion characteristics

Figure 4 shows the derivative characteristics of adhesion with respect to relative sliding. When dµ/ds<0, there is an unstable region.

Let us assume that the wheelset drive of a rail vehicle moves along a straight path in the rated torque mode. The following main operating parameters are taken into account: longitudinal relative slippage of both wheels s_0, vehicle speed v [km/h], and vertical force of the wheel N_0 (Fig.5).

These operating parameters correspond to the engine torque of a two-axle bogie with separate two-wheel drives [24]. Therefore, the traction forces of the bogie and the longitudinal adhesion forces at the wheel/rail contact have the following form:

$$M(s_0, v) = 2\mu_0 N_0 r \frac{1}{p}, \quad F_0 = 4\mu_0 N_0, \quad T_0 = \mu_0 N_0, \tag{22}$$

where $\mu_0 = \mu(s_0, v)$ is the longitudinal adhesion coefficient [15]. When the wheels of the wheelset oscillate in the wheel/rail contact, there are longitudinal adhesion forces $T_{i\,ad}$, transverse adhesion forces $A_{i\,ad}$ and adhesion moments during rotation $M_{i\,ad}$, the magnitude of which can be expressed, for example, according to [24] (index i corresponds to the designation of the nodes in which they are deployed on the axis):

$$T_{i\,ad} = \mu(s_i, v)N_i, \qquad A_{i\,ad} = b_{22}(\dot{u}_i + r\dot{\psi}_i) + b_{23}\,\dot{\vartheta}_i,$$
$$M_{i\,ad} = -b_{23}(\dot{u}_i + r\dot{\psi}_i) + b_{33}\,\dot{\vartheta}_i, \tag{23}$$

where $\dot{u}_i$ is the lateral speed (in the direction of the wheelset axle), $\dot{\vartheta}_i$ is the rotation, and $\dot{\psi}_i$ is the angular velocity of the wheel.

The actual normal force is determined using the following formula:

$$N_i = N_0 - k_R\,\dot{v}_i - b_R\,\dot{v}_i - m_R\,\ddot{v}_i.$$

In this case, adhesion coefficient $\mu(s_i, v)$ is described by dependences (20)–(21).
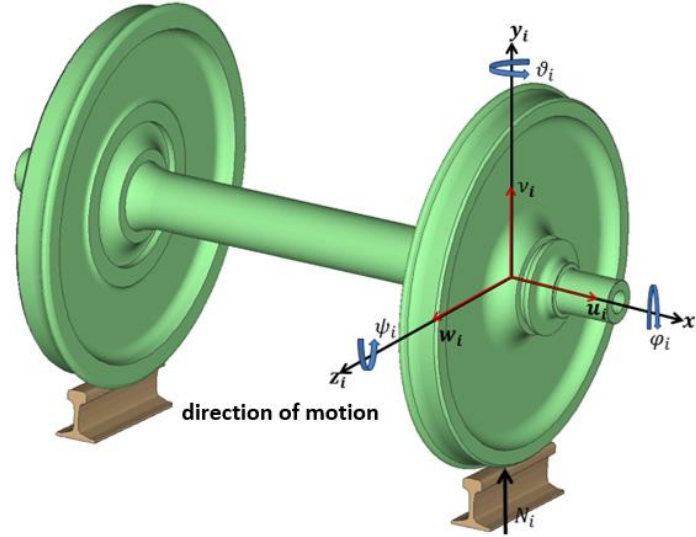
Fig. 5. Wheelset/rail contact

The relative sliding of the wheels at the speed of the locomotive v [km/h] and their torsional $\dot\varphi_i$ (around the axis of the wheelsets) and longitudinal $\dot w_i$ (in the direction of the locomotive motion) oscillations is determined by:

$$s_i = s_0 + \frac{r\dot\varphi_i - \dot w_i}{v} \cdot 3{,}6\,, \qquad s_0 = \frac{3{,}6 \cdot r\omega_D - v}{v}, \tag{24}$$

where s_0 is the relative sliding of two wheels to a failure caused by torque, r is the radius of the wheel, and ω_D is the angular velocity of the wheelsets to failure. The coefficients $b_{ij} = 3.6 \cdot \frac{f_{ij}}{v}$ correspond to the Kalker coefficients f_{ij} [25] and are calculated for a constant wheel force N_0. The vector of adhesion forces in the coordinate system $x_i\ y_i\ z_i$ (Fig. 5) has the following form:

$$\boldsymbol{f}_i^T = [-A_{i\,ad}, N_i, T_{i\,ad}, -T_{i\,ad}\,r, -M_{i\,ad}, -A_{i\,ad}r,]. \tag{25}$$

Expanding into a series of the nonlinear dependences of the adhesion coefficient on the relative sliding of the wheels, using the Taylor formula, and restricting ourselves to the first two terms of the expansion, we obtain the adhesion coefficient in a linearized form

$$\mu(s_i, v) = \mu(s_0, v) + \left[\frac{\partial\mu}{\partial s_i}\right]_{s_i=s_0}(s_i - s_0). \tag{26}$$

If we assume that $N_i = N_0$ then the longitudinal adhesion force can be expressed as:

$$T_{i\,ad} = \mu_0 N_0 + b_{11}(r\dot\varphi_i - \dot w_i), \quad b_{11} = \frac{3{,}6}{v} N_0 \left[\frac{\partial\mu}{\partial s}\right]_{s=s_0}. \tag{27}$$

Now, based on (23), (27), the adhesion force vector can be written as:

$$\boldsymbol{f}_i = -\underbrace{\begin{bmatrix} b_{22} & 0 & 0 & 0 & b_{23} & rb_{22} \\ 0 & b_R & 0 & 0 & 0 & 0 \\ 0 & 0 & b_{11} & -rb_{11} & 0 & 0 \\ 0 & 0 & -rb_{11} & r^2 b_{11} & 0 & 0 \\ -b_{23} & 0 & 0 & 0 & b_{33} & -rb_{23} \\ rb_{22} & 0 & 0 & 0 & rb_{23} & r^2 b_{22} \end{bmatrix}}_{\boldsymbol{B}_{i\,ad}} \underbrace{\begin{bmatrix} \dot u_i \\ \dot v_i \\ \dot w_i \\ \dot\varphi_i \\ \dot\vartheta_i \\ \dot\psi_i \end{bmatrix}}_{\dot{\boldsymbol{q}}_i} + \underbrace{\begin{bmatrix} 0 \\ N_0 - k_R v_i - m_R\ddot v_i \\ \mu_0 N_0 \\ -\mu_0 N_0 r \\ 0 \\ 0 \end{bmatrix}}_{\boldsymbol{f}_i}. \tag{28}$$

Accordingly, the vector of adhesion forces acting on the vibration of the wheelset has the following form:

$$\boldsymbol{f}_i = -\boldsymbol{B}_{i\,ad}\dot{\boldsymbol{q}}_i + \boldsymbol{f}_i\,. \tag{29}$$

Here, $\boldsymbol{B}_{i\,ad}$ is the matrix that contains the damping effect of line b_R.

If $\boldsymbol{B}_{i\,ad}$, $b_R = 0$ (i.e., vertical oscillations of the wheel center are not taken into account), then vector $\boldsymbol{f}_i$ has the following form:

$$\boldsymbol{f}_i = [0, N_0, \mu_0 N_0, -\mu_0 N_0 r, 0, 0]^T. \tag{30}$$

This vector expresses the load on the wheel in steady-state mode.

Now the linearized mathematical model of the wheelset contacting with the rail, can be written as a system of a second-order homogeneous differential equation, i.e.:

$$\overline{\boldsymbol{M}}\ddot{q}(t) + (\boldsymbol{B}_{ad}(s_0, v) + \boldsymbol{B}_s)\dot{q}(t) + \boldsymbol{K}q(t) = \boldsymbol{0}. \tag{31}$$

Here: $\overline{\boldsymbol{M}} = \boldsymbol{M} + \boldsymbol{M}_1^{(D)} + \boldsymbol{M}_2^{(D)}$, $\boldsymbol{K} = \boldsymbol{K}_s + \boldsymbol{K}_B$, $\boldsymbol{B}_{ad}(s_0, v) = diag(\dots \boldsymbol{B}_{i\,ad} \dots \boldsymbol{B}_{i\,ad})$.

In the case of rotating wheelsets (i.e. $when\ \omega_0 \neq 0$ rad/s) the following values are taken into account:

- wheel/rail contact, i.e. $\boldsymbol{B}_{ad}(s_0, v)$;
- damping matrix $\boldsymbol{B}_s$ as a linear combination of mass and stiffness matrices, i.e. $\boldsymbol{B}_s = a\boldsymbol{M}_s + b\boldsymbol{K}_s$.

Here, a is the mass proportionality factor and b is the stiffness proportionality factor.

To determine the eigenvalues of the linearized model of rotating wheelsets, (31) can be reduced to solving an algebraic eigenvalue problem of the following form

$$[\lambda\boldsymbol{S}(s_0, v) + \boldsymbol{A}]\boldsymbol{u} = \boldsymbol{0} \tag{32}$$

in the state space, i.e. $\boldsymbol{u}(t) = [\dot{q}^T(t) \quad q^T(t)]^T$, $\boldsymbol{u}(t) \in \boldsymbol{R}^{2n}$ given by the following matrices

$$\boldsymbol{S}(s_0, v) = \begin{bmatrix} \boldsymbol{0} & \overline{\boldsymbol{M}} \\ \overline{\boldsymbol{M}} & (\boldsymbol{B}_{ad}(s_0, v) + \boldsymbol{B}_s) \end{bmatrix}, \qquad \boldsymbol{A} = \begin{bmatrix} -\overline{\boldsymbol{M}} & \boldsymbol{0} \\ \boldsymbol{0} & \boldsymbol{K} \end{bmatrix}. \tag{33}$$

The eigenvalues λ of equation (32) are a pair complex quantity, i.e. $\lambda = \omega = \omega_R \pm i\omega_I$ and their imaginary part is the eigenfrequencies ω_I in rad/s of the rotating wheelsets. The conjugate root $\bar{\lambda} = \omega = \omega_R - i\omega_I$ corresponds to every complex root $\lambda = \omega = \omega_R + i\omega_I$ of the characteristic equation (32).

If the real parts of all roots of the characteristic equation (32) are negative ($\omega_R < 0$, $\omega_I > 0$), then the unperturbed motion is asymptotically stable.

If among the roots of the characteristic equation there is at least one real root (i.e., a positive one ($\omega_R > 0$, $\omega_I > 0$)), then the unperturbed motion is unstable [27].

To illustrate it, Table 2 shows the first eight natural frequencies of equation (32).

Table 2. Natural frequencies of rotating wheelsets

Number of eigen frequencies	Complex natural frequencies of wheelsets for $s_0 = 0.009, v = 40$ km/h	Damping coefficients	Complex natural frequencies of wheelsets for $s_0 = 0.014, v = 40\ km/h$	Damping coefficients
1	$-2.33e - 09 \pm 0.0i$	0.0	$-3.85e - 08 \pm 0.0i$	0.0
2,3	$-2.10 \pm 57.79i$	0.036	$-2.10 \pm 57.79i$	0.036
4	$-17.21 \pm 78.20i$	0.220	$0.35 \pm 80.07i$	-0.004
5,6	$-16.81 \pm 162.71i$	0.103	$-16.81 \pm 162.71i$	0.103
7,8	$-78.79 \pm 345.26i$	0.228	$-78.79 \pm 345.26i$	0.228

The first eight pairs of complex-pair eigenvalues, ordered by the magnitude of the imaginary part, are presented in Table 2. Positive real parts of eigenvalues (i.e. $0.35 \pm 80.07i$) reflect the instability of the system. This instability corresponds to the positive real part of the complex-pair eigenvalues (i.e. $0.35 \pm 80.07i$ for $s_0 = 0.014, v = 40$ km/h). However, the wheelset of the rolling stock works stably, mainly in the linear area of the adhesion characteristic (Fig. 3), but despite this, even at a speed of $v = 40$ km/h, and $s_0 \approx 0.009$ the perturbed motion of the wheelsets with the rail turned out to be stable.

Conclusions

1. A mathematical model was developed to evaluate the dynamic characteristics of rolling stock wheelsets, taking into account the viscoelastic properties of the material using the Boltzmann–Volterra hereditary theory of viscoelasticity.

2. A method and algorithm were developed for determining the natural frequencies, modes and decrement of oscillations of wheelsets taking into account the dissipation in the system and the viscoelastic properties of the material.

3. Eigenfrequencies, modes and decrement of vibrations of wheelsets were determined for various viscoelastic parameters of the material, and the independence of the logarithmic decrement of vibrations of the system from the number of natural frequencies was revealed.

4. A mathematical model was developed to evaluate the dynamic characteristics of wheelsets in contact with the rail taking into account damping in the form of a linear combination of the mass and stiffness matrices of the system.

5. The natural frequencies, modes and decrement of vibrations of the wheelsets of the rolling stock with the rail were determined, taking into account the slippage of the wheels and the speed of the rail vehicle. The positive real parts of the complex-pair eigenvalues which reflected the instability of the system were identified. With this mathematical model, it became possible to establish the stability of the unperturbed motion of wheelsets together with the rail in almost any area of the adhesion characteristic.

References

1.   Xincan J. Experimental and numerical modal analyses of high-speed train wheelsets. *Journal of Rail and Rapid Transit*. 2014;230(3): 643-661.

2.   Jian H, Shuoqiao Z, Xinbiao X, Zefeng W, Guotang Z, Xuesong J. High-speed wheel/rail contact determining method with rotating flexible wheelset and validation under wheel polygon excitation. *Vehicle System Dynamics*. 2017;56(8): 1233-1249.

3.   Balekwa BM, Kallon DVV. Correlation of Short Pitch Rail Corrugation with Railway Wheel-Track Resonance at Low Frequencies of Excitation. *Vibration.* 2020;3(4): 491-520.

4.   Zhong S, Xiong J, Xiao X, Wen Z, Jin X. Effect of the first two wheelset bending modes on wheel-rail contact behavior. *Journal of Zhejiang University Science A*. 2014;15(12): 984-1001.

5.   Baeza L, Giner-Navarro J, Thompson DJ, Monterde J. Eulerian models of the rotating flexible wheelset for high frequency railway dynamics. *Journal of Sound and Vibration*. 2019;449: 300-314.

6.   Chaar N, Berg M. Experimental and numerical modal analyses of a loco wheelset. *Veh Syst Dyn.* 2004;41: 597 – 606.

7.   Chaar N, Berg M. Vehicle-Track Dynamic Simulations of a Locomotive Considering Wheelset Structural Flexibility and Comparison with Measurements. *Journal of Rail and Rapid Transit*. 2005;219(4): 225-238.

8.   Pong B, Simon D, Iwnicki P. The influence of wheelset flexibility on polygonal wear of locomotive wheels. *Wear.* 2019;102917: 432-433.

9.   Ribeiro D, Calçada R, Delgado R, Brehm M, Zabel V. Finite-element model calibration of a railway vehicle based on experimental modal parameters. *International Journal of Vehicle Mechanics and Mobility*. 2013;51(6): 821-856.

10.   Quynh LV, Jianrun Z, Liem NV, Cuong BV, Long LX, Phuong DT. Experimental modal analysis and optimal design of cab's isolation system for a single drum vibratory roller. *Vibroengineering PROCEDIA*. 2020;31: 52-56.

11.   Carlos C, Asier A, Ibon E. Simple flexible wheelset model for low-frequency instability simulations. *Journal of Rail and Rapid Transit*. 2012;228(2): 169-181.

12.   Xiaoxuan Y, Gongquan T, Wei L, Zefeng W. On the formation mechanism of high-order polygonal wear of metro train wheels: Experiment and simulation. *Engineering Failure Analysis*. 2021;127: 105512.
13.   Mpho P, Daramy V, Bingo M, Michele C. Design and Modeling of Viscoelastic Layers for Locomotive Wheel Damping. *Vibration*. 2021;4: 906–937.
14.   Ahmedov O, Mirsaidov M. Finite element of rotating wheelset and its natural frequencies determination. *Materials Physics and Mechanics*. 2021;47(5): 706-719.
15.   Mirsaidov M, Boytemirov M, Yuldashev F. Estimation of the Vibration Waves Level at Different Distances. In: Akimov P, Vatin N. (eds) *Proceedings of FORM 2021. Lecture Notes in Civil Engineering*. Springer; 2022. p.207-215.
16.   Mirsaidov M., et all. Eigenwaves propagation in three-layer cylindrical viscoelastic shells with a filler non-uniform in thickness. IOP Conf. Series: Materials Science and Engineering. 2021; 1030(1):1-17. doi:10.1088/1757-899X/1030/1/012074.
17.   Mirsaidov, M., Vatin, N., Abdikarimov, R., Khodzhaev, D., Normuminov, B. Parametric Vibrations of Viscoelastic Rectangular Plates with Concentrated Masses. Proceedings of STCCE 2021. Lecture Notes in Civil Engineering. 2021; 169(1):72-79. https://doi.org/10.1007/978-3-030-80103-8_8.
18.   Mirsaidov, M., Safarov, I., Boltayev, Z., Teshaev, M. Spread waves in a viscoelastic cylindrical body of a sector cross section with cutouts. IOP Conference Series: Materials Science and Engineering. 2020; 869 (2020) 1-11. doi:10.1088/1757-899X/869/4/042011.
19.   Mirsaidov M., et all. Dynamics of structural - inhomogeneous coaxialmulti-layered systems "cylinder-shells". Journal of Physics. 2020; 1706 (2020):1-15. doi:10.1088/1742-6596/1706/1/012033.
20.   Mirsaidov, M., Teshaev, M., Ablokulov, S., Rayimov, D. Choice of optimum extinguishers parameters for a dissipative mechanical system. IOP Conference Series: Materials Science and Engineering. 2020; 883 (2020):1-12. doi:10.1088/1757-899X/883/1/012100
21.   Filatov AN. *Asymptotic Methods and Theory of Differential and Integro-Differential Equations*. Tashkent: Fan; 1974.
22.   Ilyushin AA, Pobedrya BE. *Fundamentals of the mathematical theory of thermo-visco-elasticity*. Moscow: Nauka; 1970. (In Russian)
23.   Lata M. Modelování přechodových dějů v torzním systému pohonu hnacího vozidla, *Scientific Papers of the University of Pardubice, Series B - The Jan Perner Transport Faculty*. 2003;2: 45-58.
24.   Zeman V, Hlaváč Z. Dynamic wheelset drive load of the railway vehicle caused by short-circuit motor moment. *Applied and Computational Mechanics*. 2009;3(2): 423-434.
25.   Grag V, Dukkipati, R. *Dynamics of railway vehicle systems*. London Academic Press; 1984.
26.   Mirsaidov M, Abdikarimov R, Khudainazarov S, Sabirjanov T. Damping of high-rise structure vibrations with viscoelastic dynamic dampers. *E3S Web of Conferences*. 2020;224: 1-14.
27.   Merkin DR. *Introduction to the theory of motion stability*. Science; 1987.

THE AUTHORS

Ahmedov Olimjon (iD)
e-mail: olimjon84@mail.ru

Mirsaidov Mirziyod (iD)
e-mail: mirsaidov1948@mail.ru